Università degli Studi di Padova

Dipartimento di Ingegneria dell'Informazione

Corso di Laurea Triennale in Ingegneria dell'Informazione

IMU calibration without mechanical equipment

(Calibrazione di IMU svincolata da apparati meccanici)

Laureando

David Tedaldi

Relatore

Prof. Emanuele Menegatti

Correlatore

Ing. Alberto Pretto

23 settembre 2013

Anno Accademico 2012/2013

Abstract

In this thesis, I propose a robust and easy to implement method to calibrate an IMU without any external equipment. The procedure is based on a multi-position scheme, providing scale and misalignments factors for both the accelerometers and gyroscopes triads, while estimating the sensor biases. The method only requires the sensor to be moved by hand and placed in a set of different, static positions (attitudes). I describe a robust and quick calibration protocol that exploits an effective parameterless *static filter* to reliably detect the static intervals in the sensor measurements, where local stability of the gravity's magnitude is assumed. First the accelerometers triad is calibrated taking measurement samples in the static intervals. Then these results are exploited to calibrate the gyroscopes, employing a robust numerical integration technique.
The performances of the proposed calibration technique has been successfully evaluated via extensive simulations and real experiments with a commercial IMU provided with a calibration certificate as reference data.

Abstract - Italian Version

In questa tesi propongo un metodo robusto e facile da implementare per calibrare un IMU senza apparecchiature esterne. La procedura si basa su uno schema a più posizioni, fornendo fattori di scala e di disallineamento sia per la triade di accelerometri che per quella di giroscopi, stimando contemporaneamente i bias dei sensori. Il metodo richiede solo che il sensore venga spostato a mano e posto in una serie di diverse posizioni statiche (oreintato i diversi modi). Si descrive un protocollo di calibrazione robusta e veloce che sfrutta un efficace filtro statico *per rilevare in modo affidabile gli intervalli statici nelle misure dei sensori e dove si assume un alta stabilità locale dell'intensità della forza di gravità. Dapprima si calibra la triade di accelerometri prendendo campioni di misura negli intervalli statici, sfruttando poi questi risultati per calibrare i giroscopi, impiegando una robusta tecnica di integrazione numerica. Le prestazioni della tecnica di calibrazione proposta sono state valutate con successo attraverso vaste simulazioni ed esperimenti reali con un IMU commerciale fornito con un certificato di calibrazione come dati di riferimento.*

Contents

Chapter 1

Introduction

"Accidere ex una scintilla
incendia passim."

"Sometimes,
from a single spark,
a fire breaks out."

Lucrezio

1.1 Motivation

IMUs (Inertial Measurement Units) are very popular sensors in robotics: among others, they have been exploited for inertial-only navigation [1], attitude estimation [2], and visual-inertial navigation [3, 4], also using a smartphone device [5]. IMUs used in robotics are usually based on MEMS (micro electro mechanical systems) technology. They are composed by a set of tri-axial clusters: an accelerometers, a gyros and often a magnetometer cluster. In an ideal IMU, the tri-axial clusters should share the same 3D orthogonal sensitivity axes that span a three dimensional space, while the scale factor should convert the digital quantity measured by each sensor into the real physical quantity (e.g, accelerations and gyro rates). Unfortunately, low cost MEMS based IMU are usually affected by non accurate scaling, sensor axis misalignments, cross-axis sensitivities, and non zero biases. The IMU calibration refers to the process of identify these quantities.

Many commercial IMU in the cost range form 1000 $ to 2000 $, such as the Xsens MTi [6] exploited in the experiments (Sec. 4), are factory calibrated[1].

[1] Often they are also compensated over temperature

Each sensor is sold with its own calibration parameters set stored into the firmware or inside a non-volatile memory, providing accurate measurements off the shelf. Unfortunately, the overhead cost for the factory calibration is predominant: usually the sensor hardware (sensors, chips, embodiment, ...) is likely to be only a fraction of the final device cost. Actually, the factory calibration is usually performed using standard but effective methods, where the device outputs are compared with known references: this process requires time for each sensor and a high cost equipment. On the other hand, low-cost IMUs (20-100 $) and the IMU sensors that equip current smartphones are usually poorly calibrated, resulting in measurements coupled with not negligible systematic errors. For instance, state-of-the-art visual-inertial navigation systems such the one presented in [5], that exploits a smartphone as experimental platform, while performing so well in forward, almost regular, motion[2], shows lower performances in more "exciting" motions, i.e. in motions that quickly change linear acceleration and rotational axes.
In this thesis, it is propose an effective and easy to implement calibration scheme, that only requires to collect IMU data with the simple procedure described in the flow chart reported in Fig. 1.1. After an initial initialization period with no motion, the operator should move the IMU in different positions, in order to generate a set of distinct, temporarily stable, rotations. The collected dataset is used to calibrate the scale and misalignments factors for both the accelerometers and gyroscopes triads, while estimating the sensor biases. As other calibration technique, the effect of the cross-axis sensitivities is neglected, since for minor misalignments and minor cross-axis sensitivities errors it is usually difficult to distinguish between them.
The presented procedure exploits the basic idea of the multi-position method, firstly presented in [7] for accelerometers calibration: in a static position, the norms of the measured accelerations is equal to the magnitudes of the gravity plus a multi-source error factor (i.e., it includes biases, misalignment, noise,...). All these quantities can be estimated via minimization over a set of static attitudes. After the calibration of the accelerometer triad, we can use the gravity vector positions measured by the accelerometers as a reference to calibrate the gyroscope triad. Integrating the angular velocities between two consecutive static positions, we can estimate the gravity positions in the new orientation. The gyroscopes calibration is finally obtained minimizing the errors between these estimates and the gravity references given by the calibrated accelerometers.

[2]Actually, during an almost regular motion miscalibration errors may easily be assimilated by the biases included in the system state

In this procedure the gyroscopes calibration accuracy strongly depends on the accuracy of the accelerometers calibration, being used as a reference. Moreover, signal noise and biases should negatively affect both the calibration accuracy and the reliability of the algorithms used to detect the actual static intervals used in the calibration. Finally, a consistent numerical integration process is essential to mitigate the effect of the signal discretization, usually sampled at 100 Hz. In this approach, these problems are faced introducing the following modifications to the standard multi-position method:

- The proposed calibration protocol exploits a larger number of static states with reduced periods, in order to increase the cardinality of the dataset while preserving the assumption of local stability of the sensors biases
- As proposed in [8], we characterize the gyroscope bias drifts in a period estimated using the Allan variance
- A simple but effective *static detector* is introduced, it exploits the sensor noise magnitude, a fixed-time sampling window and a cutting threshold, automatically estimated inside the optimization framework
- The Runge-Kutta numerical integration method id employed to improve the accuracy of the gyroscope calibration.

The system is extensively tested using synthetic data affected by variable biases, misalignments, scale factor errors, and noise. In all of the cases, stable and accurate results are obtained. Moreover, the calibration of a commercial, factory calibrated Xsens MTi IMU, is performed using its raw, uncalibrated, data as input. Calibration results are comparable to the factory parameters reported by the device's calibration certificate.

1.2 Releted Works

Traditionally the calibration of an IMU has been done by using special mechanical platforms such as a robotic manipulator, moving the IMU with known rotational velocities in a set of precisely controlled orientations [9, 10, 11]. At each orientation, the output of the accelerometers are compared with the precomputed gravity vector while during the rotations the output of gyroscopes are compared with the precomputed rotational velocity. However, the mechanical platforms used for calibration are usually very expensive, resulting in a calibration cost that often exceeds the cost of the IMU's hardware.

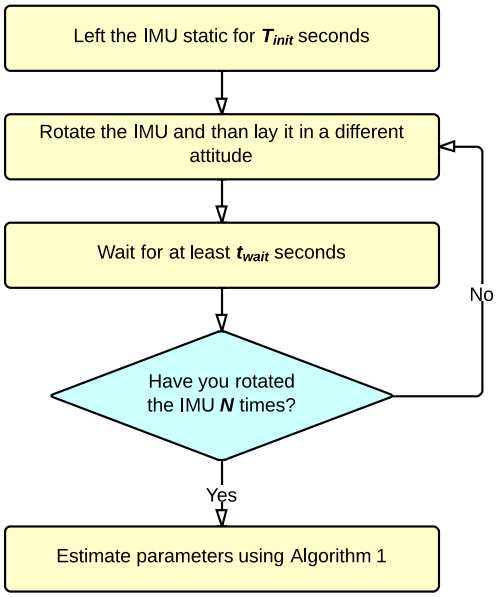

Figure 1.1: Calibration protocol.

In [12] a calibration procedure that exploits a marker-based optical tracking system has been presented, while in [13], the GPS readings are used to calibrate initial biases and misalignments. Clearly, the accuracy of these method strongly depends on the accuracy of the employed kinematic reference (i.e., the motion capture system or the GPS). The multi-position method was firstly introduced by Lotters *et al.* [7]: authors proposed to calibrate the biases and the scale factor of the accelerometers using the fact that the magnitude of the static acceleration must equal to the gravity's magnitude. This technique has been extended in [14] and [15] to include the accelerometer axis misalignment. The error model they proposed for the gyroscopes is similar to the one used for the accelerometers, but the calibration procedure in this case requires a single axis turntable to provide a strong rotation rate signal, providing high calibration accuracy. Unfortunately, these approaches not only requires a mechanical equipment, but the two triads are independently calibrated, and the misalignment between them can't be detected. In [8] and [16] authors presented two calibration schemes that don't require any external mechanical equipment. Similarly to the approach exposed in this thesis, in the first work authors calibrate the accelerometers exploiting the high local stability of the gravity vector's magnitude, and then gyroscopes calibration is obtained comparing the gravity vector sensed by the calibrated accelerometer with the gravity vector obtained by integrating the angular

velocities. In the second work authors also exploit the local stability of the magnetic field.
Hwangbo *et al.* [17] recently proposed a self-calibration technique based on an iterative matrix factorization: using gravity as accelerometers reference and a camera as gyroscopes reference.

1.3 Goals

This study's aim is to provide the basis for developing algorithm for a easy to perform cheap-IMU calibration without external equipment, thus obtaining smartphone's *IMU* calibrated by the user himself, making possible high quality visual-inertial navigation and Structure form Motion[3] (*SfM*) in smartphones.

We devolop an algorithm based on the latest works on this field, especially on [8] , and we define some simple rules that a potential user should follow to calibrate well an *IMU*. In this work, we test the validity of the algorithm with a large set of simulations, and thus we give the results about the accurancy of the calibration. We also provide the results of a real experimentation done using an MTi *IMU* [18] by Xsens [6] comparing our calibration to the component's datasheet.

1.4 Structure of the Thesis

First the description of an IMU, the description of the uncalibrated state problems and the concept of a calibration is discussed in Chapter Two, including mathematical models. In Chapter Three, the algorithm treaty is described including the theoretical background. In Chapter Four is described in detail the experiments carried out, simulations and real experiment, and all results are reported and commented. Finally, in chapter five conclusions are drawn on the work done and future work are exposed.

[3] *SfM* refers to the process of estimating three-dimensional structures from two-dimensional image sequences which may be coupled with local motion signals.

Chapter 2

Theoretical Background

"Das Studium und allgemein das Streben nach Wahrheit
und Schönheit ist ein Gebiet,
auf dem wir das ganze Leben lang Kinder bleiben dürfen."

"The study as the pursuit of truth and beauty
is a sphere of activity in which
we are permitted to remain children all our lives."

Albert Einstein

2.1 Inertial Measurement Unit

An Inertial measurement unit (IMU) is used in order to know the attitude of the body where it is assembled on. It consists on clusters of accelerometers and gyroscopes, sometimes also magnetometers. It works by detecting the current rate of acceleration using the acceleromters' cluster, and detects changes in rotational attributes like pitch, roll and yaw using the gyroscopes's cluster. The magnetometer, which serves to measure the magnetic field, it is used mostly to assist the calibration against orientation's drift.
In this work, like in [12] and in [8, 14], only accelerometer and gyroscope are considered, and so the model which is used is like the one pictured in Fig. 2.1. How it is possible to see in Fig. 2.1, the Inertial measurement unit consists of two clusters of sensors, the accelerometers' one and the gyroscopes' one. Each cluster has three elements, one for each axis of the orthogonal reference system.

There are many types of accelerometers and gyroscopes but for what concerns this thesis, the IMU's components are MEMS technology based. This kind of components are particularly suitable for robotics application

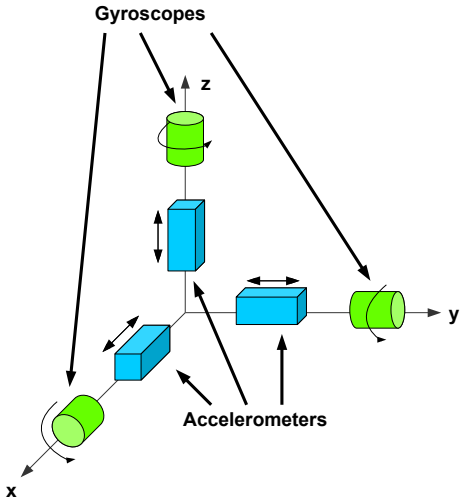

Figure 2.1: Simplified Scheme of an IMU

because of their small size and inexpensive nature. MEMS, acronym for Micro Electro Mechanical Systems, is the integration of mechanical elements, sensors, actuators, and electronics on a common silicon substrate through the utilization of microfabrication technology [19]. The fondamental idea behind MEMS is to combining together silicon-based microelectronics with micromachining technology to form the so called systems-on-a-chip [20].

2.2 Uncalibrated State

It was said that MEMS based IMU are very interesting, because of their small size, they are cheap and they have a very low power consumption too, but it is needed to calibrate them to make their output useful in practice. Infact there are lots of imperfections due to sensors themselfs, to the soldering of the sensor on the chip, and to other reasons that cause data distortion so that the unit's output become useless.
The sensor model describes the process of measurement from the actual physical quantity to the sensor voltage output. The same linear model is used for accelerometers as gyroscopes. It accounts for scale, misalignment, non-orthogonality and bias errors. Similar models are used also in [8, 14, 16] and in [21, 22].

2.2.1 Misalignment and Non-Orthogonality Errors

For an ideal IMU, the 3 axes of the accelerometers triad and the 3 axes of the gyroscopes triad define a single, shared, orthogonal 3D frame. Each accelerometer senses the acceleration along one of the distinct axis, while each gyroscope measures the angular velocity around one of the same axes. Unfortunately in real IMUs, due to assembly inaccuracy, the two triads form two distinct (i.e., misaligned), non-orthogonal, frames.

As introduced above, both the accelerometers frame (AF) and the gyroscopes frame (GF) are usually non-orthogonal. Two associated orthogonal, ideal frames (AOF and GOF, respectively) are defined in the following way:

- The x-axis of the AOF and the one of the AF coincide
- The y-axis of the AOF lies in the plan spanned by the x and y axes of the AF.

For the gyroscopes case, it is sufficient to substitute the AF and AOF acronyms with GF and GOF, respectively. Finally, a body frame (BF) is defined, this is an orthogonal frame that represents, for example, the coordinate frame of the IMU's chassis. The body frame usually differs from the AF and GF frames by small angles but, in general, there is no direct relation between them.
For small angles, a measurements $\mathbf{s}^S$ in a non-orthogonal frame (AF or GF) can be transformed in the orthogonal body frame as:

$$\mathbf{s}^B = \mathbf{T}\mathbf{s}^S, \qquad \mathbf{T} = \begin{bmatrix} 1 & -\beta_{yz} & \beta_{zy} \\ \beta_{xz} & 1 & -\beta_{zx} \\ -\beta_{xy} & \beta_{yx} & 1 \end{bmatrix} \tag{2.1}$$

where $\mathbf{s}^B$ and $\mathbf{s}^S$ denote the specific force (acceleration), or equivalently the rotational velocity, in the body frame coordinates and accelerometers (or gyroscopes) coordinates, respectively. Here β_{ij} is the rotation of the *i-th* accelerometer or gyroscope axis around the *j-th* BF axis, see Fig. 2.2.

On the other hand, the two orthogonal frames BF and AOF (and, equivalently, BF and GOF) are relate by a pure rotation.
In the presented calibration method, it is assumed that the body frame BF coincides with the accelerometers orthogonal frame AOF: in such case, the angles $\beta_{xz}, \beta_{xy}, \beta_{yx}$ become zero, so in the accelerometers case Eq. 2.1 becomes:

$$\mathbf{a}^O = \mathbf{T}^a\mathbf{a}^S, \qquad \mathbf{T}^a = \begin{bmatrix} 1 & -\alpha_{yz} & \alpha_{zy} \\ 0 & 1 & -\alpha_{zx} \\ 0 & 0 & 1 \end{bmatrix} \tag{2.2}$$

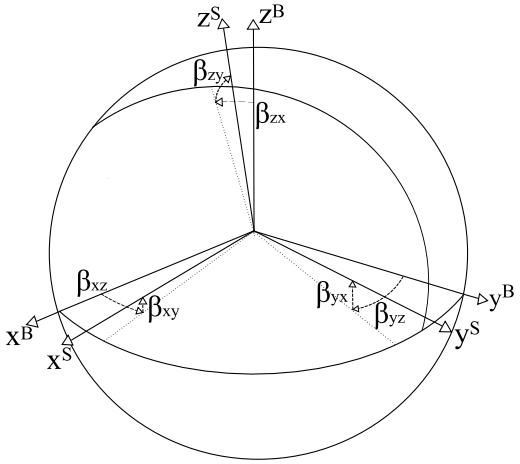

Figure 2.2: Sensor (acceleromter or gyroscopes) sensitivity axes x^S, y^S, z^S, and body frame coordinates axes x^B, y^B, z^B.

where letter β, referring to the general case, are changed with the letter α, referring to the accelerometer case, while $\mathbf{a}^O$ and $\mathbf{a}^S$ denote the specific acceleration in AOF and AF, respectively[1].
It is possible to see this simplification from an other point of view: we are just orthogonalizing the sensitivity coordinates frame of the accelerometer, without aligning it with the real body coordinates frame, the one we should know. Acting in such a way obviously it is lost the information about the real orientation of what it will be the calibrated coordinate frame.
Since in the practical situations where the proposed calibration is thought to be used it is impossible to fix with sufficient precision any component, with known orientation and absolute position, here the goal is just to calibrate as precisely as possible the IMU, meaning that it is obtained an orthogonal, unitary scaling factor aligned system, leaving the "absolute position-oreintation" problem to the solver of the specific problem in wich the IMU is used.

For example in [23] they investigate the visual inertial structure from motion problem with special focus on its observability properties. They mathematically demonstrate that considering a system consisting of a monocular camera and IMU, the extrinsic camera-IMU calibration is observable. In [3, 24] they describe an ego-motion estimation system based on aforementioned system, in which they are able to identify the rotation matrix, $\mathbf{R}$, and

[1]To relate the obtained calibration with a different body frame (e.g. BF'), it is sufficient to estimate the rotation matrix that relate AOF to BF', for instance using the accelerometers outputs in three different orthogonal orientations.

the translational one, $\mathbf{T}$, between the camera and the IMU.

Talking about the gyroscopes sensitivity coordinates frame we can not do the same simplification. This is because we want to obtain calibrated measurement coherent between the gyroscopes and the accelerometers. Thus we have to orthogonalize the gyroscopes' sensitivity coordinate frame and we also have to align it to the accelerometers' sensitivity coordinate frame, rotating it. Then, for the gyroscopes, we have

$$\boldsymbol{\omega}^O = \mathbf{T}^g \boldsymbol{\omega}^S, \qquad \mathbf{T}^g = \begin{bmatrix} 1 & -\gamma_{yz} & \gamma_{zy} \\ \gamma_{xz} & 1 & -\gamma_{zx} \\ -\gamma_{xy} & \gamma_{yx} & 1 \end{bmatrix} \tag{2.3}$$

where $\boldsymbol{\omega}^O$ and $\boldsymbol{\omega}^S$ denote the specific angualr velocities in the orthogonal coordinates frame and IMU's gyroscopes sensitivity coordinates frame, respectively. $\mathbf{T}^g$ is the matrix that permit to orthogonalize the gyroscopes sensitivity axis, and aligne it to the accelerometers' sensitivity axis.

In the ideal case both $\mathbf{T}^a$ and $\mathbf{T}^g$ are the identity matrix.

2.2.2 Scaling Error and bias

Talking about the scaling error and the presence of bias, both the accelerometers and the gyroscopes are treated in the same way. Two scaling matrix are introduced

$$\mathbf{K}^a = \begin{bmatrix} s_x^a & 0 & 0 \\ 0 & s_y^a & 0 \\ 0 & 0 & s_z^a \end{bmatrix}, \qquad \mathbf{K}^g = \begin{bmatrix} s_x^g & 0 & 0 \\ 0 & s_y^g & 0 \\ 0 & 0 & s_z^g \end{bmatrix}. \tag{2.4}$$

In the ideal case both $\mathbf{K}^a$ and $\mathbf{K}^g$ are the identity matrix. Also two bias vector are introduced

$$\mathbf{b}^a = \begin{bmatrix} b_x^a \\ b_y^a \\ b_z^a \end{bmatrix}, \qquad \mathbf{b}^g = \begin{bmatrix} b_x^g \\ b_y^g \\ b_z^g \end{bmatrix}. \tag{2.5}$$

In the ideal case both $\mathbf{b}^a$ and $\mathbf{b}^g$ are a 3×1 null vector.

2.2.3 Complete Sensor Error Model

To complete the sensor error model the measurement noise is considered too. Thus the complete models are

$$\mathbf{a}^O = \mathbf{T}^a \mathbf{K}^a (\mathbf{a}^S + \mathbf{b}^a + \boldsymbol{\nu}^a) \tag{2.6}$$

for the accelerometers, and

$$\boldsymbol{\omega}^O = \mathbf{T}^g\mathbf{K}^g(\boldsymbol{\omega}^S + \mathbf{b}^g + \boldsymbol{\nu}^g) \tag{2.7}$$

for the gyroscopes. Where $\boldsymbol{\nu}^g$ and $\boldsymbol{\nu}^g$ are the accelerometer measurement noise and the gyroscope measurement noise, respectively.

2.3 Calibration

There are several different kind of methods for calibrating the IMU. In this section we give a look at these methods starting from the calibration based entirely on mechanical equipment, continuing with the first attempt to ease the procedures reducing the equipment needed then finishing with the approach we based our study on.

2.3.1 Mechanical Equipment based Calibration

In [10] they say: *"Calibration is the process of comparing instrument outputs with known reference information and determining coefficients that force the output to agree with the reference information over a range of output values"*.
Having the opportunity to compare data collected from IMU to data coming from highly controlled movements the unknown parameters of the considered sensor error model can be identified using simply linear least squares algorithm.

In [21] they present a device that simplifies and speeds up the calibration process of the accelerometers and gyroscopes removing the need to reposition the IMU manually during the calibration process. They designed and realize the device to calibrate a specific Inertial Measurement Unit, but the same idea could be potentially implemented to calibrate other IMUs. The device consist on a mechanical gimbal system with three actuated degrees of freedom. For the accelerometers, the calibration is done by positioning the IMU to known orientations and for the gyroscopes by rotating the IMU at several constant speeds around specified axis. Based on these measurements, the optimal parameters for the sensor error model are calculated using linear least squares.

2.3.2 Semi-Mechanical Calibration

In [14] Skog and Händel propose an approach for calibrating a low-cost IMU requiring no mechanical platform for the accelerometer calibration and

only a rotating table for the gyro calibration. The proposed calibration methods utilize the fact that ideally the norm of the measured output of the accelerometers and gyroscopes clusters are equal to the magnitude of applied force and rotational velocity, respectively.
Obviously the norm of the gyroscopes output is compared to the known magnitude of the rotational velocity of the rotating table. For what concerns the acceleromters the norm of the cluster output is compared to the magnitude of the apparent gravity force.

2.3.3 Calibration Without External Equipment

The basic principle of this type of calibration, proposed in [8] and then retracted and extended to the calibration of the magnetometer in [16], consists of calibrating the accelerometers as in the calibration viewed in Sec. 2.3.2, and then calibrate the gyroscopes comparing the outputs of the accelerometer and the IMU orientation integration algorithm, after arbitrary motions. The properties used and proposed cost function allow the gyroscopes to be calibrated without external equipment, such as a turntable, or requiring precise maneuvers. We discuss and analyze this approach further in Ch. 3 while explaining the procedure proposed in this thesis.

2.4 Quaternions

Now we introduce quaternions because they are a powerful tool to parametrize rotation matrices. There are many sources to draw upon information on quaternions so we will introduce them very briefly and speak directly on how they are used to describe rotations in three dimensions [28, 29].

The set of complex numbers, $\mathbb{C}$, can be simply defined as

$$\mathbb{C} = \mathbb{R} + \mathbb{R}i, \qquad with \qquad i^2 = -1. \tag{2.8}$$

In this sense, complex number generalize real numbers. In a similar way quaternions (or *Hamilton's Numbers*) generalize complex number. The set of quaternions, $\mathbb{H}$, is defined as

$$\mathbb{H} = \mathbb{C} + \mathbb{C}j, \qquad with \qquad j^2 = -1 \qquad and \qquad i \cdot j = -j \cdot i. \tag{2.9}$$

Sometimes for semplicity of notationij is denoted by k. And so we have that an element content in $\mathbb{H}$ is in the form

$$\mathbf{q} = q_0 + q_1 i + (q_2 + q_3 i)j = q_0 + q_1 i + q_2 j + q_3 ij = q_0 + q_1 i + q_2 j + q_3 k \tag{2.10}$$

where q_0, q_1, q_2, $q_3 \in \mathbb{R}$. From Eq. 2.9 we can see that the product of i and j is anticommutative, thus in general the product between two quaternions is not commutative. Now we consider a particular subset of quaternions: the unit quaternions, that is

$$\mathbb{S}^3 = \{\mathbf{q} \in \mathbb{H} \mid q_0^2 + q_1^2 + q_2^2 + q_3^2 = 1\}. \tag{2.11}$$

The set of unit quaternions is simply the unit-radius origin-centered sphere in $\mathbb{R}^4$. Any rotation in three dimensions can be represented as a combination of an axis and a rotation angle. Quaternions represent a simple way to encode this axis-angle representation in four numbers and apply the rotation corresponding to a position vector that represents a point relative to the origin in $\mathbb{R}^3$. Through the euloero formula we can represent a rotation as

$$\mathbf{q} = e^{\frac{1}{2}\theta(v_x i + v_y j + v_z k)} = cos\frac{1}{2}\theta + sin\frac{1}{2}\theta(v_x i + v_y j + v_z k) \tag{2.12}$$

where θ is the rotation angle and $\mathbf{v} = (v_x, v_y, v_z)$ is a versor which rapresents the rotation axis. Now consider $\mathbf{q} = (a, b, c, d)$ a unit quaternion rapresenting a rotation, we can get the rotation matrix as follows

$$\mathbf{R}^q = \begin{bmatrix} a^2 + b^2 - c^2 - d^2 & 2bc - 2ad & 2bd + 2ac \\ 2bc + 2ad & a^2 - b^2 + c^2 - d^2 & 2cd - 2ab \\ 2bd - 2ac & 2cd + 2ab & a^2 - b^2 - c^2 + d^2 \end{bmatrix} \tag{2.13}$$

Finally we give the definition of the product between to quaternions, but before we introduce a new notation. Given a quaternion $\mathbf{q} = a + bi + cj + dk$, we divide it into two different parts, a scalar one (a) and a vectorial one ($\mathbf{v} = bi + cj + dk$). So we have $\mathbf{q} = a + \mathbf{v}$.
Given this new notation we can express the product between quaternions using the usual vectorial and scalar product we are familiar with. Considered that $i^2 = j^2 = k^2 = ijk = -1$ the product can be written as

$$(s + \mathbf{v})(t + \mathbf{w}) = (st - \mathbf{vw})(s\mathbf{w} + t\mathbf{v} + \mathbf{v} \times \mathbf{w}) \tag{2.14}$$

where it is clear that the product is not commutative for the presence of the vectorial product.

2.4.1 Integration Algorithm

It is possibile to consider each gyriscope's sample as constant over period of time equal to the sampling period. This first order approximation permits to compute the overall rotation associated to a set of gyroscope's samples

just using a moltiplication chain of matrices. In general this approximation does not give sufficiently precise results and for the proposed method we use the a fourth order numerical integration algorithm we further discussed in Sec. 3.4.2. In spite of it is unused we explain how this first order algorithm works, because it permits to understand more intuitively the higher order algorithm.

If there is a series of rotations in a certain order, it is possible to compute the total rotation by properly multiplying the quaternions associated with each rotation. Let $(r_1, r_2, ..., r_n)$ be an ordered set of rotations parametrized by matrices $(\mathbf{R}_1, \mathbf{R}_2, ..., \mathbf{R}_n)$ and, $(\mathbf{q}_1, \mathbf{q}_2, ..., \mathbf{q}_n)$ the corrispondent ordered set of quaternions, thus the total rotation r_{tot} is

$$r_{tot} \qquad \leftrightarrow \qquad \mathbf{R}_{tot} \qquad \leftrightarrow \qquad \mathbf{q}_{tot} = \mathbf{q}_n \mathbf{q}_{n-1} \cdot ... \cdot \mathbf{q}_2 \mathbf{q}_1 \tag{2.15}$$

where we used Eq. 2.13 to obtain $\mathbf{R}_{tot}$ from $\mathbf{q}_{tot}$.

Chapter 3

Algorithm

"Quando le cose diventano troppo complicate, qualche volta
ha un senso fermarsi e chiedersi:
ho posto la domanda giusta?"

"When things get too complicated, sometimes
it makes sense to stop and ask:
I asked the right question?"

Enrico Bombieri

The magnetometer's data are not used because in the context we are considering, the smarphone's IMU calibration, distortions due to metallic structures and antennas could be excessive to be properly considered by a linear model.

3.1 Fundamentals Properties

The two fundamental hypothesis which permit to set up the calibration method are taken from [8]. They impose physical and mathematical constraints on the sensor outputs, thus the two properties are used to calibrate the sensors instead of relying on values coming from high physical precision mechanical equipments. In this way the *IMU* can be easily calibrated by the users in the field.

The first property permits to calibrate the accelerometer cluster, and it is **Property-1** : *the magnitude of the static acceleration measured must equal that of the gravity.*

This is the constraint applied to the triaxial accelerometer which imposes a correlation between the axis, or in other words the values measured on each axis are not indipendent.

The second property, the one we use to calibrate the gyroscope cluster, is **Property-2** : *the gravity vector measured using a static triaxial accelerometer must equal the gravity vector computed using the IMU orientation integration algorithm, which in turn uses the angular velocities measured using the gyroscopes, and it starts the orientation integration from a direction given by the static triaxial accelerometer itself.*
This property must hold whenever the IMU is static after any arbitrary motion.

3.2 Acceleromter Cost Function

The accelerometer calibration consists on the estimation of all the 9 unknown parameters of the sensor error model presented in Sec. 2.2.3. That is

$$\mathbf{a}^O = \begin{bmatrix} 1 & -\alpha_{yz} & \alpha_{zy} \\ 0 & 1 & -\alpha_{zx} \\ 0 & 0 & 1 \end{bmatrix} \begin{bmatrix} s_x^a & 0 & 0 \\ 0 & s_y^a & 0 \\ 0 & 0 & s_z^a \end{bmatrix} \left(\mathbf{a}^S + \begin{bmatrix} b_x^a \\ b_y^a \\ b_z^a \end{bmatrix} \right). \tag{3.1}$$

Thus the unknown parameter vector for the accelerometer ($\boldsymbol{\theta}^{acc}$) which is estimated is

$$\boldsymbol{\theta}^{acc} = \left[\alpha_{yz}, \alpha_{zy}, \alpha_{zx}, s_x^a, s_y^a, s_z^a, b_x^a, b_y^a, b_z^a \right]. \tag{3.2}$$

So we can define the funtion

$$\mathbf{a}^O = h(\mathbf{a}^S, \boldsymbol{\theta}^{acc}) = \mathbf{T}^a \mathbf{K}^a (\mathbf{a}^S + \mathbf{b}^a). \tag{3.3}$$

$||\mathbf{g}||$ is defined as the actual magnitude of the local gravity vector that can be easily recovered from specific public tables (e.g., knowing latitude, longitude and altitude of the location where we are performing the calibration). Then the cost function which is minimized is

$$\mathbf{L}(\boldsymbol{\theta}^{acc}) = \sum_{k=1}^{N} (||\mathbf{g}||^2 - ||h(\mathbf{a}_k^S, \boldsymbol{\theta}^{acc})||^2)^2 \tag{3.4}$$

where N is the number of sets of measurement from which they are extracted acceleration vectors $\mathbf{a}_k^S$ (measured in the non-orthogonal AF), averaging the accelerometers readings in a temporal window inside each static interval. In order to minimize Eq. 3.4 the *Levenberg-Marquardt* (LM) algorithm is used with initial guess $\boldsymbol{\theta}_0^{acc} = \left[0, 0, 0, 1, 1, 1, 0, 0, 0\right]$, which rapresents the ideal case.

3.3 Gyroscope Cost Function

For what concerns gyroscopes we bring back the system to a new bias-free system simply averaging the static gyroscope signals (this sentence is further discussed in Sec. 3.4.3). And so 9 parameters have to be estimated like in the accelerometer case. That is

$$\boldsymbol{\omega}^O = \begin{bmatrix} 1 & -\gamma_{yz} & \gamma_{zy} \\ \gamma_{xz} & 1 & -\gamma_{zx} \\ -\gamma_{xy} & \gamma_{yx} & 1 \end{bmatrix} \begin{bmatrix} s_x^g & 0 & 0 \\ 0 & s_y^g & 0 \\ 0 & 0 & s_z^g \end{bmatrix} \left(\boldsymbol{\omega}^S\right). \tag{3.5}$$

Thus the unknown parameter vector for the gyroscope ($\boldsymbol{\theta}^{gyro}$) which is estimated is

$$\boldsymbol{\theta}^{gyro} = \left[\gamma_{yz}, \gamma_{zy}, \gamma_{xz}, \gamma_{zx}, \gamma_{xy}, \gamma_{yx}, s_x^g, s_y^g, s_z^g\right]. \tag{3.6}$$

Ψ is the operator that converts a sequence of $\boldsymbol{\omega}_i^S$, from i = 0 to i = n, for some n, and the initial gravity vector $\mathbf{u}_0$, to the gyroscope computed gravity vector $\mathbf{u}_g$

$$\mathbf{u}_g = \Psi\left[\omega_i^S, \mathbf{u}_0\right] \tag{3.7}$$

where Ψ can be any algorithm that computes the orientation through integrating the angular velocities ω_i^S (we describe more precisely Ψ in Sec. 3.4.2).

Having given all these definitions we can define the cost function we minimize

$$\mathbf{L}(\boldsymbol{\theta}^{gyro}) = \sum_{k=1}^{N} ||\mathbf{u}_{a,k} - \mathbf{u}_{g,k}||^2 \tag{3.8}$$

where N is the number of sets of measurement, $\mathbf{u}_{a,k}$ and $\mathbf{u}_{a,k}$ are the *k-th* acceleration vector measured in the calibrated accelerometer frame and the *k-th* acceleration vector computed using gyroscope frame respectively. To minimize Eq. 3.8 the LM algorithm is used with initial guess $\boldsymbol{\theta}_0^{gyro} = \left[0, 0, 0, 0, 0, 0, 1, 1, 1\right]$, which rapresents the ideal case.

3.4 Calibration Procedure

As introduced in Sec. 1, the proposed calibration framework requires to collect a dataset with the stream of raw accelerometers and gyroscopes readings, taken while the operator moves the IMU in different static positions, in order to generate a set of distinct, temporarily stable, rotations. A simple diagram of our calibration protocol is reported in Fig. 1.1. As mentioned in Sec. 3.2, to mitigate the noise effect in the minimization of Eq. 3.4, so it is needed to average the signals over a suitable time interval. This impose a

lower bound in the lengths of the static interval (t_{wait} in Fig. 1.1). A initialization period (T_{init} in Fig. 1.1) with no motion is essential as well: this will be exploited to characterize the gyroscopes biases (Sec. 3.4.3) and the static detector operator (Sec. 3.4.1).

3.4.1 Static Detector

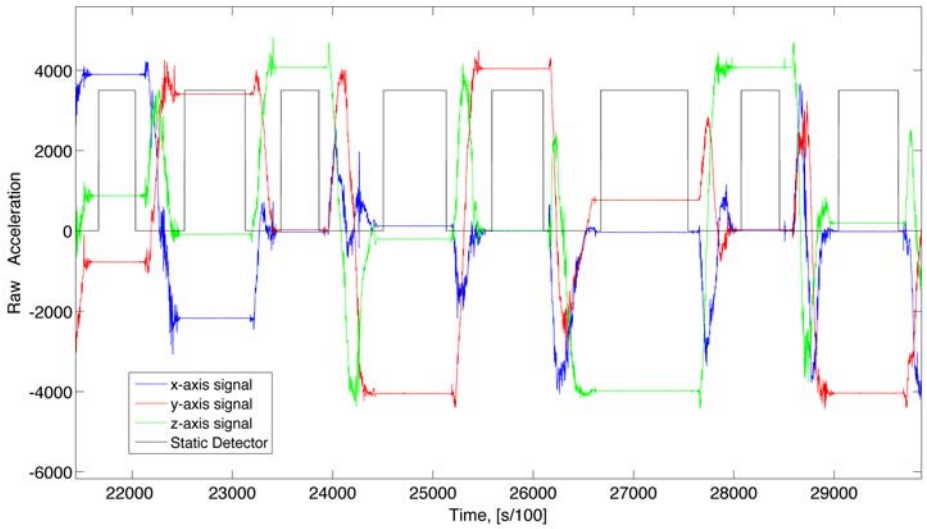

Figure 3.1: An example of the static detector applied to the real raw accelerometers' data: the static detector is represented by the black square wave, its high level classify an interval as static.

The accuracy of the calibration strongly depends on the reliability in the classification between static and motion intervals: to calibrate the accelerometers static intervals are used, while for gyroscopes calibration they are also included the motion intervals between two consecutive static intervals. In my experience, band-pass filter based operators, like the *quasi-static detector* used in [8], perform poorly with real datasets: detected static intervals frequently includes some small portion of motion. Moreover, they require a fine tuning, since they depend on three parameters. The parameters are the two frequecy caracterizing the pass-band based filter and the threshold used to cut the signal. Actually this latter parameter is automaticcaly estimated by their calibration algorithm, but the other two must be tuned by the operator. Here it is proposed instead to use a variance based static detector operator, that exploits the lower bound in the lengths of the static interval introduced above. This detector is based on the accelerometer signals: given a time

interval of length t_{wait} seconds (see Fig. 1.1), for each accelerometers sample $(\mathbf{a}_y^t, \mathbf{a}_y^t, \mathbf{a}_y^t)$ at time t, the variance magnitude is computed as:

$$\varsigma(t) = \sqrt{[var_{t_w}(\mathbf{a}_x^t)]^2 + [var_{t_w}(\mathbf{a}_y^t)]^2 + [var_{t_w}(\mathbf{a}_z^t)]^2} \tag{3.9}$$

where $var_{t_w}(\mathbf{a}^t)$ is an operator that compute the variance of a general signal $\mathbf{a}^t$ in a time interval of length t_w seconds centered in t. We classify between static and motion intervals simply checking if the square of $\varsigma(t)$ is lower or greater then a threshold. As a threshold, we consider an integer multiple of the square of the variance magnitude ς_{init}, computed over all the initialization period T_{init}. In all the experiments, we use $t_w = 1\ s$, while T_{init} is estimated using the Allan variance (see Sec. 3.4.3). It is important to note that the proposed static detector does not require any parameter tuning: the integer multiplier used classify the signal, which is the unique parameter, is automatically estimated by our calibration algorithm (see Sec. 3.5). In Fig. 3.1 is reported an example of how our static filter works on real data: in this case the estimated integer multiplier is 6.

3.4.2 Runge-Kutta Integration

As reported in Eq. 3.7, in the gyroscopes calibration we need to perform a discrete time angular velocity integration: a robust and stable numerical integration method is desirable since it can improve the calibration accuracy. Given a common instruments rate of 100 Hz (like the Xsens MTi IMU used in the experiments) and since we represent rotations using quaternion arithmetic, with this setup a proper integration algorithm choice [25] is the *Runge-Kutta* 4^{th} *order normalized method* (RK4n).
Let Eq. 3.10 be the differential equation describing the quaternion kinematics:

$$\mathbf{f}(\mathbf{q}, t) = \dot{\mathbf{q}} = \frac{1}{2}\boldsymbol{\Omega}(\boldsymbol{\omega}(t))\mathbf{q} \tag{3.10}$$

where $\boldsymbol{\Omega}(\boldsymbol{\omega})$ is the operator which turns the considered tri-dimensional angular velocity into the real skew symmetric matrix representation, that is:

$$\boldsymbol{\Omega}(\boldsymbol{\omega}) = \begin{bmatrix} 0 & -\omega_x & -\omega_y & -\omega_z \\ \omega_x & 0 & \omega_z & -\omega_y \\ \omega_y & -\omega_z & 0 & \omega_x \\ \omega_z & \omega_y & -\omega_x & 0 \end{bmatrix}. \tag{3.11}$$

It is possible to compute the overall rotation associated to a set of gyroscope's samples using RK4n integration algorithm in this way:

$$\mathbf{q}_{k+1} = \mathbf{q}_k + \Delta t \frac{1}{6} \left(\mathbf{k}_1 + 2\mathbf{k}_2 + 2\mathbf{k}_3 + \mathbf{k}_4 \right), \tag{3.12}$$

$$\mathbf{k}_i = \mathbf{f}(\mathbf{q}^{(i)}, t_k + c_i \Delta t), \tag{3.13}$$

$$\mathbf{q}^{(i)} = \mathbf{q}_k, \qquad for\ i = 1, \tag{3.14}$$

$$\mathbf{q}^{(i)} = \mathbf{q}_k + \Delta t \sum_{j=1}^{i-1} a_{ij} \mathbf{k}_j, \qquad for\ i > 1. \tag{3.15}$$

Where $\mathbf{q}_k$ is the quaternion parametrization of the rotation associated to the first k samples of the gyro's measurement set. All the coefficients needed, c_i and a_{ij}, are

$$\begin{gathered} c_1 = 0, \quad c_2 = \tfrac{1}{2}, \quad c_3 = \tfrac{1}{2}, \quad c_4 = 1, \\ a_{21} = \tfrac{1}{2}, \quad a_{31} = 0, \quad a_{41} = 0, \\ a_{32} = \tfrac{1}{2}, \quad a_{42} = 0, \quad a_{43} = 1. \end{gathered}$$

Finally, for each step, we also need to normalize the $(k+1)$-th quaternion.

$$\mathbf{q}_{k+1} \rightarrow \frac{\mathbf{q}_{k+1}}{||\mathbf{q}_{k+1}||}. \tag{3.16}$$

3.4.3 Allan Variance

The random gyroscope bias drifts are characterized using the Allan variance ([26], [8]), which measures the variance of the difference between consecutive interval averages. The Allan variance σ_a^2 is defined as:

$$\sigma_a^2 = \frac{1}{2} \left\langle (x(\tilde{t}, k) - x(\tilde{t}, k-1))^2 \right\rangle = \frac{1}{2K} \sum_{k=1}^{K} (x(\tilde{t}, k) - x(\tilde{t}, k-1))^2 \tag{3.17}$$

where $x(\tilde{t}, k)$ is the k-th interval average which spans $\tilde{t}$ seconds, and K is the number of interval which the total considered time is segmented in. We compute the Allan variance for each gyroscope axis, with $t_0 \leq \tilde{t} \leq t_n$. We fix $t_0 = 1s$, $t_n = 225s$. The time in which the Allan variances of the three axis converge to a small value represents a good choice for initialization period T_{init} (Fig. 1.1). In this initialization period, we compute the average of the static gyroscope signals to correctly determine the gyroscopes biases used in the calibration.
In the case of the Xsens MTi IMU, a good value for T_{init} is 50 seconds (see Fig. 3.2).

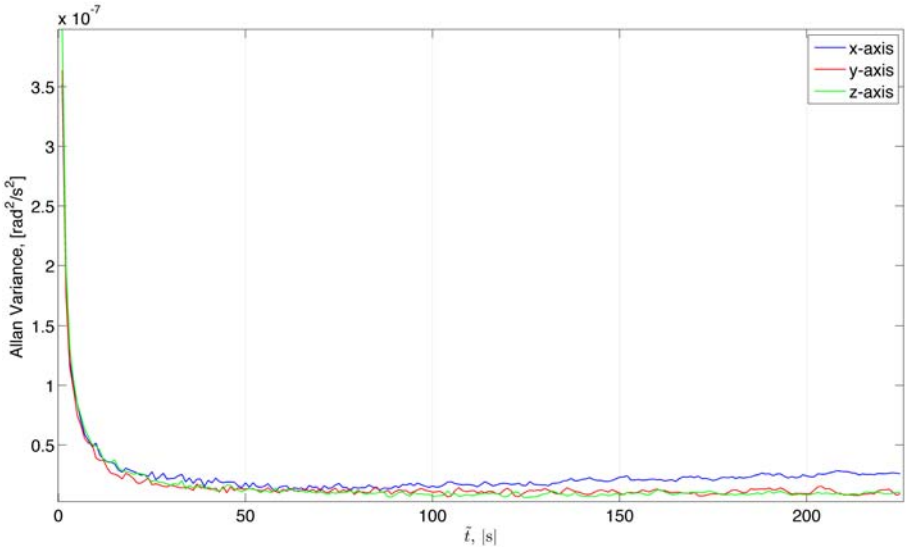

Figure 3.2: Allan Variance computed for the Xsens MTi gyroscopes triad.

3.5 Complete Procedure

To avoid unobservability in the calibration parameters estimation, a minimum of nine different attitudes [15] has to be collected (e.g., Fig. 3.3). In our experience, a higher number N of distinct attitudes are required to get better calibration results, while keeping reduced the duration of each static interval in order to preserve the assumption of temporal stability of the gyroscopes biases. With $36 \leq N \leq 50$ and $1\ s \leq t_{wait} \leq 4\ s$, we obtain a good trade-off between calibration accuracy, biases stability, and noise reduction. The duration of the initialization period T_{init} is given by the Allan variance analysis (see Sec. 3.4.3). The calibration protocol is summarized in Fig. 1.1, while in Algorithm 1 the pseudo-code of the calibration algorithm is reported.

Algorithm 1 IMU Calibration

Require: T_{init}, t_{wait}; $\mathbf{a}^S$ and $\boldsymbol{\omega}^S$ (accelromter's and gyroscope's dataset collected according to the protocol summarized in Fig. 1.1).

$\mathbf{b}^g \leftarrow$ average gyroscope signals over T_{init};
$\boldsymbol{\omega}^S_{biasfree} \leftarrow \boldsymbol{\omega}^S$ - $\mathbf{b}^g$;
$M_{inf} \leftarrow$ empty matrix;
$\varsigma_{init} \leftarrow$ Eq. 3.9, with $t_w = T_{init}$;
for $i = 1 : k$
  $threshold \leftarrow i * \varsigma^2_{init}$;
  $static\_intervals \leftarrow$ static detector computed using t_{wait} and $threshold$;
  $[Residual, Params] \leftarrow$ optimize Eq. 3.4, using $static\_intervals$ and $\mathbf{a}^S$ averaging with t_{wait};
  $M_{inf}(i) \leftarrow [Residual, Params, threshold, static\_intervals]$;
end
$index_{opt} \leftarrow$ index of the minimum residual in M_{inf};
$Params_{acc} \leftarrow$ from M_{inf} using $index_{opt}$;
$static\_intervals_{opt} \leftarrow$ from M_{inf} using $index_{opt}$;
$\mathbf{a}^O \leftarrow$ calibrate $\mathbf{a}^S$ using $Params_{acc}$;
$Parameters_{gyro} \leftarrow$ optimize Eq. 3.8, using $static\_intervals_{opt}$, $\boldsymbol{\omega}^S_{biasfree}$ and $\mathbf{a}^O$ averaging with t_{wait}.

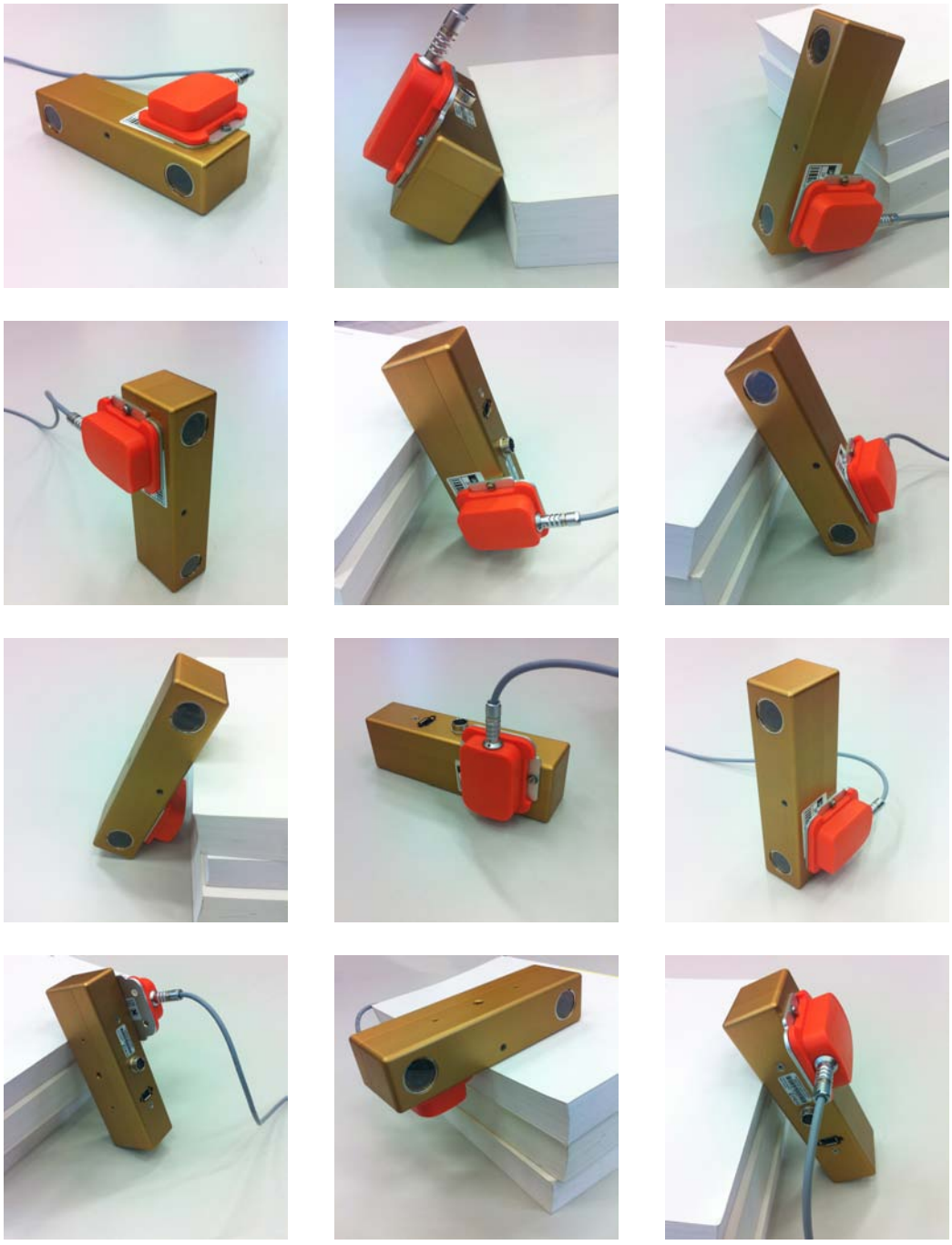

Figure 3.3: Calibration protocol: Some examples of the Xsens MTi IMU, attached to a Point Grey Bumblebee 2 stereo camera, [32], disposed in different attitudes as required by the proposed method.

Chapter 4

Experimentation

"Life is an experiment
in large part
I have not yet tried."

Henry David Thoreau

4.1 Simulations

To test our method we first do simulations. These have the advantage that the results are comparable with a perfect ground truth, the unnoisy undestorted signal and the calibration matrices we know since we generate them.
We first generate a set of ideal, nuisance free signals. The accelerometers readings are generated starting from a three-dimensional signal based on three different-pulsation sinusoids randomly modulated. At the beginning we add 5000 zero samples (the initialization period) and every time the three signals are simultaneously zero we introduce 400 zero samples (the static intervals). The three dimensional gravity vector projected onto the three axis has been added as well.
For the angular velocities sensed by the gyroscope, the idea is to consider a tri-dimensional angular velocity vector $\boldsymbol{\omega}$, which describes the perceived rotation of the aforementioned gravity vector, and then project $\boldsymbol{\omega}$ onto the three axis of the gyroscope. In this way we correlate the measurement of the two different clusters of sensors. For each motion interval different randomly zenith and azimuth velocities are chosen while for the rest of the time these velocities are considered to be equal to zero. The sampling frequency of the whole synthetic data has been fixed to 100 Hz.

For each ideal signal, we add a white gaussian noise and finally we distort the data with random generated distortion parameters, i.e.:

$$\mathbf{a}^S_{synth} = (\mathbf{T}^a\mathbf{K}^a)^{-1}\,\mathbf{a}^O_{synth} - \mathbf{b}^a \tag{4.1}$$

for the accelerations, and:

$$\boldsymbol{\omega}^S_{synth} = (\mathbf{T}^g\mathbf{K}^g)^{-1}\,\boldsymbol{\omega}^O_{synth} - \mathbf{b}^g \tag{4.2}$$

for the angular velocities. $\mathbf{a}^S_{synth}$ and $\mathbf{a}^O_{synth}$ are the synthetic acceleration in the non-orthogonal sensor frame and in the associated orthogonal frame, respectively. $\boldsymbol{\omega}^S_{synth}$ and $\boldsymbol{\omega}^O_{synth}$ are the synthetic angular velocities in the non-orthogonal sensor frame and in the associated orthogonal frame, respectively. Eq. 4.1 and Eq. 4.2 are obtained from models proposed in Eq. 2.6 and in Eq. 2.7 respectively.

In next pages we have some examples that show how much sundry can be the genereted signals. Some osservations are necessary:

- Fig. 4.1 is paired with Fig. 4.5, as Fig. 4.2 is paired with Fig. 4.6 and so on;
- the four pairs of distorted signals are genereted using four different parameters' sets of distortion. This can be easily seen in figures picturing angular velocities, where bias are very different from a instance to an other;
- the noise seems to be much bigger in angular velocities then in accelrations, but it is not properly the truth. Actually, in the real cases, the accelerometers are ususally less noisy then gyroscpes, but the difference in the figures depicting accelerations and angular velocities is due to the ordinate axis' scale.

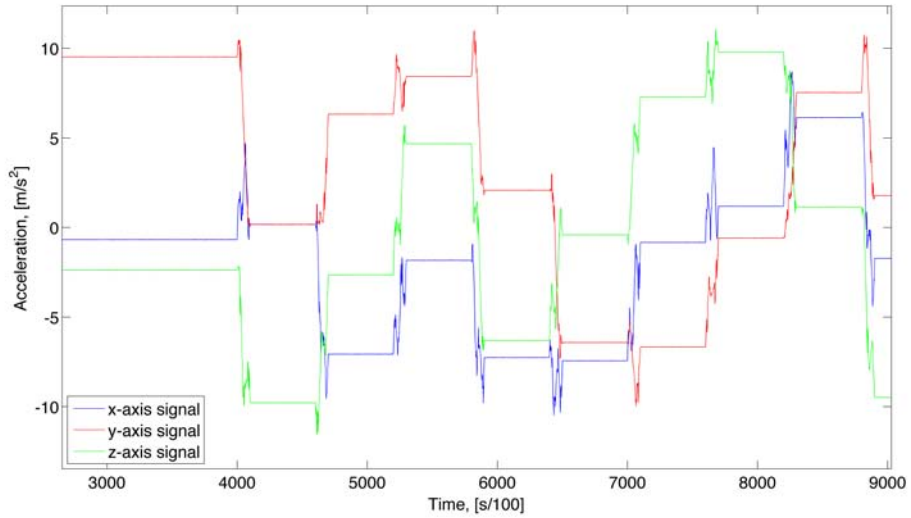

Figure 4.1: First example of acceleromter's synthetic signals.

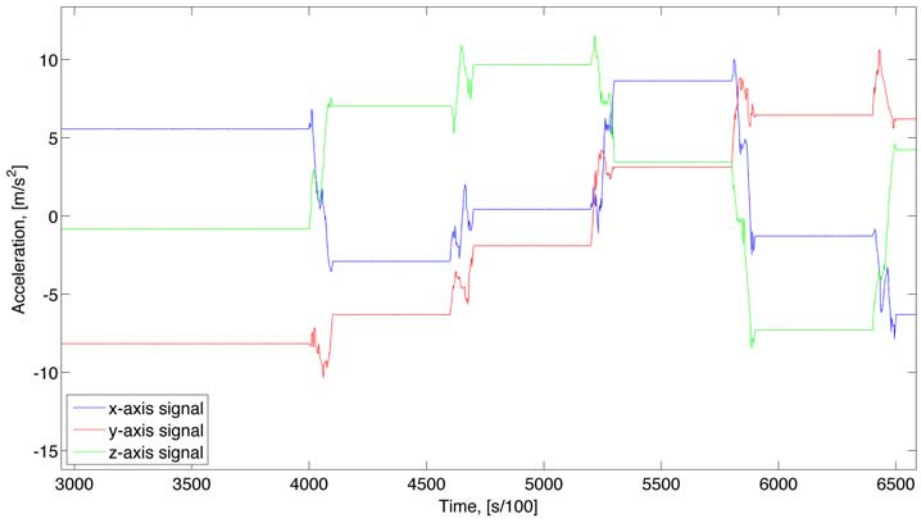

Figure 4.2: Second example of acceleromter's synthetic signals.

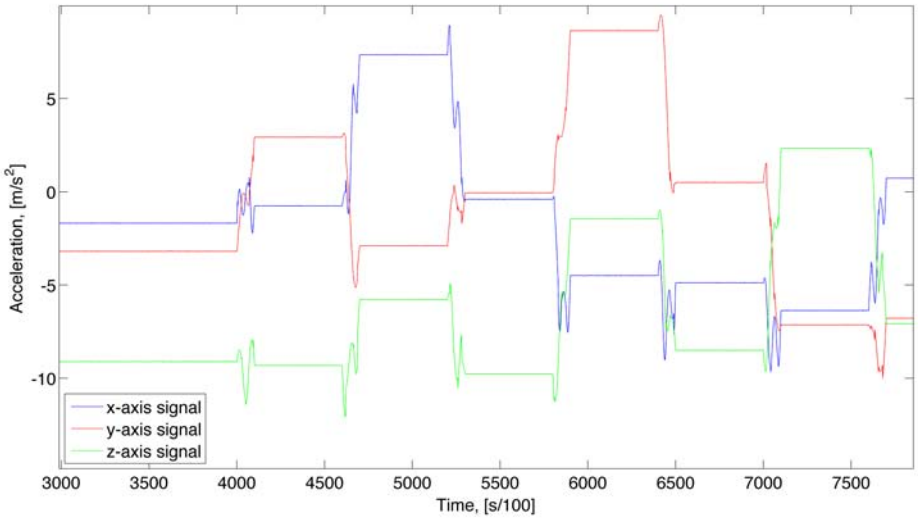

Figure 4.3: Third example of acceleromter's synthetic signals.

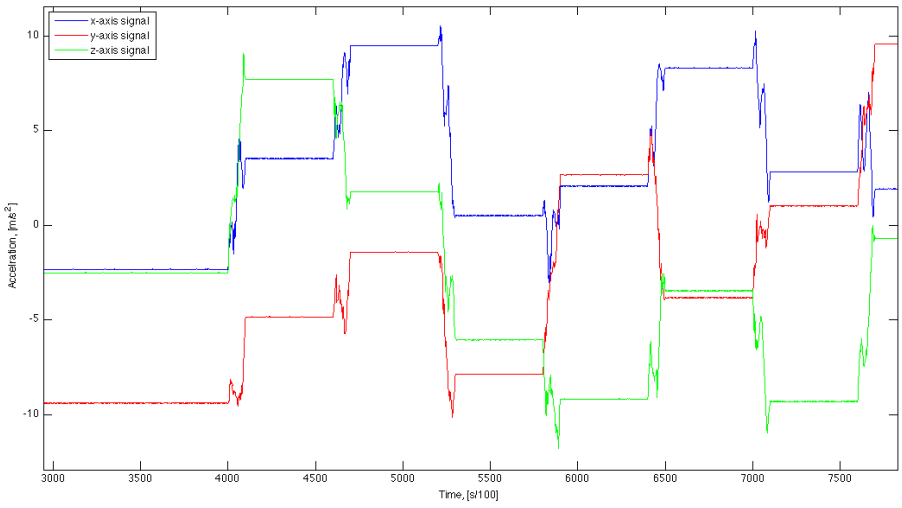

Figure 4.4: Fourth example of acceleromter's synthetic signals.

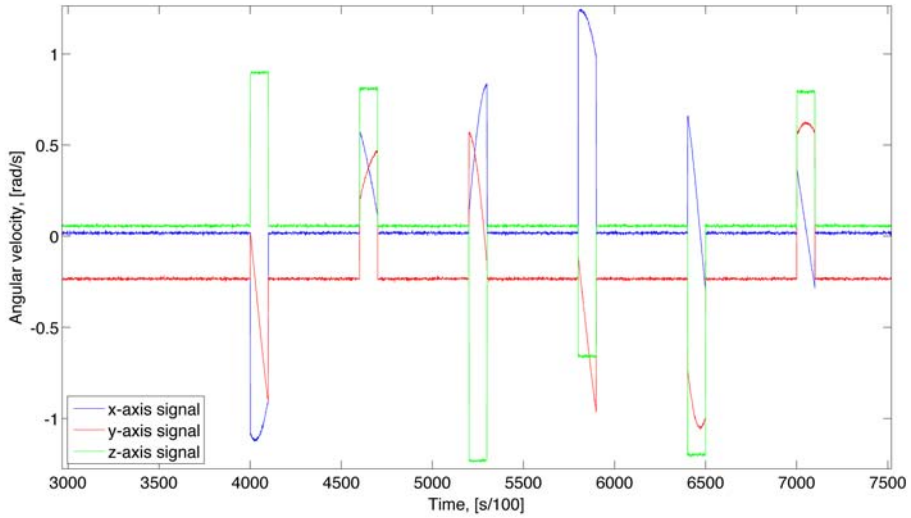

Figure 4.5: First example of gyroscope's synthetic signals.

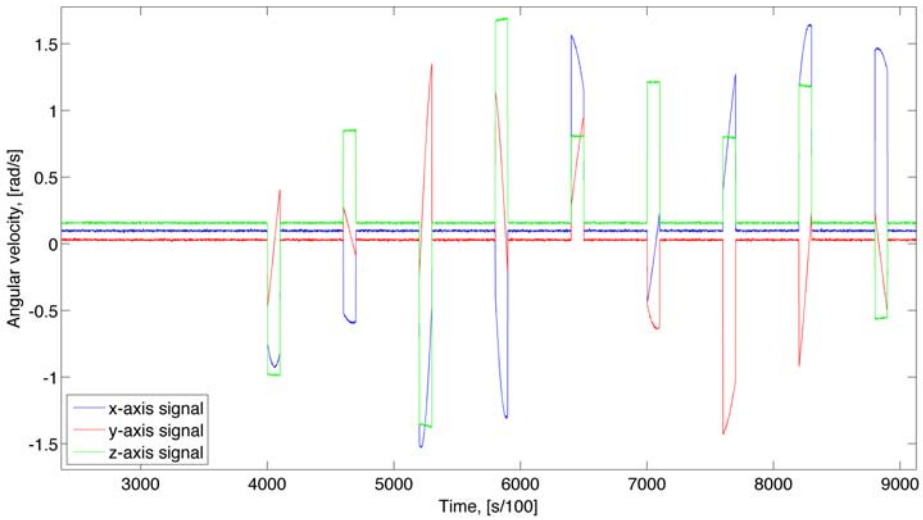

Figure 4.6: Second example of gyroscope's synthetic signals.

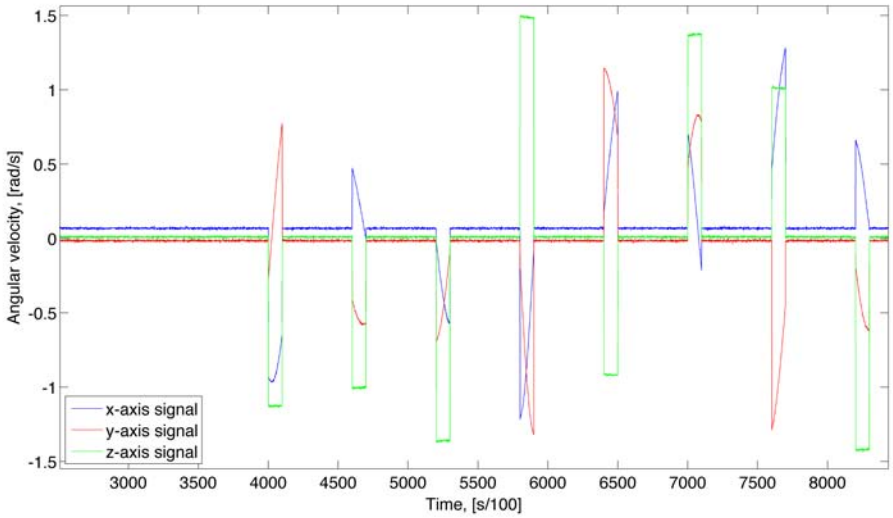

Figure 4.7: Third example of gyroscope's synthetic signals.

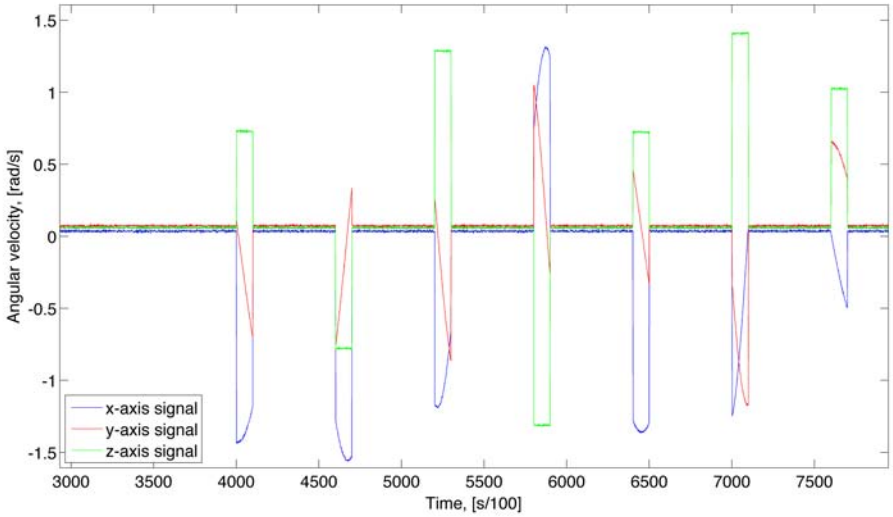

Figure 4.8: Fourth example of gyroscope's synthetic signals.

It shown in Fig. 4.9 how the *static detector* can appear. The static detector is superimposed to the tri-dimensional synthetic accelration signal over which it is computed.

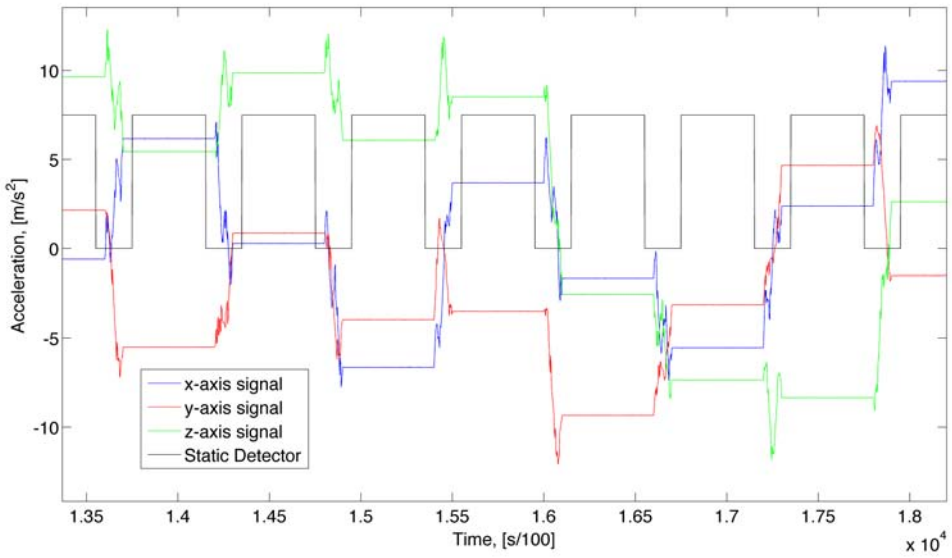

Figure 4.9: *Static detector* superimposed on accelerometer synthetic signals.

4.1.1 Evaluation Metrics

We need some metrics that allow us to evaluate the quality of our results.

In the case of the simulation, as we said before, there is the ground truth of the perfect, unnoisy, undistorted signals and the matrices and vectors we used to distort the signal. Thus the considered metrics are:

1. Comparing the estimated values to the real ones;

2. Comparing the average difference between the perfect, noise-free and undistorted signal with the noisy signal before and after calibration;

3. For the accelerometers only we give the difference between the magnitude of the gravity vector and the magnitude of the sensed acceleration as the magnitude of divergence between the sensed acceleration and the applied one. Since the magnitude of the gravity vector is assumed to be the only quantity known, the angular error here is calculated for the worst case, where the full error appears on a single accelerometer

axis which is perfectly horizontal, *i.e.* perpendicular to the gravity vector. An error of $\mathbf{g} \cdot sin(\theta_{div}^{acc})$ will result in the pitch or roll angle being measured as θ_{div}^{acc} radiants instead of zero;

4. For the gyroscopes only: we consider the magnitude and the angular error between the acceleration sensed by the calibrated accelerometer and the acceleration computed integrating the angular velocities given by the gyroscope.

4.1.2 Simulation Results

To obtain significant results from simulations, fourty different distortion parameter sets are generated. Each distortion parameter set is estimated using the proposed algorithm applied to a set of thirty randomly genereated signals which are distorted using the considered distortion parameter set.
It is computed for each distortion parameter set the mean and the variance of estimated parameters, the mean and the varience of error committed on each parameter, followed by the metrics aforementioned in Sec. 4.1.1 averaged on the thirty different results. Then the worst case is given, considered the worst since it has the biggest error on the accelerometer divergence. In fact if the accelerometer's calibration has big errors, the gyroscope's one, that is based on it, will have big errors too.
Here only one case is reported.

Table 4.1: Accelerometers Parameters. Set:1.

	Real	Mean Value	RSM x10^{-3}	Mean Erorr x10^{-3}	RSM x10^{-3}	Worst case
α_{yz}	0.0049	0.0049	0.0481	0.0398	0.0275	0.0049
α_{zy}	-0.0055	-0.0055	0.0401	0.0334	0.0214	-0.0055
α_{zx}	0.0079	0.0079	0.0296	0.0248	0.0190	0.0079
s_x^a	0.9908	0.9908	0.0327	0.0265	0.0191	0.9908
s_y^a	1.0068	1.0068	0.0304	0.0258	0.0199	1.0068
s_z^a	1.0066	1.0066	0.0215	0.0178	0.0151	1.0066
b_x^a	0.0793	0.0793	0.1369	0.1163	0.0819	0.0792
b_y^a	-0.0024	-0.0024	0.2138	0.1760	0.1178	-0.0026
b_z^a	0.0636	0.0636	0.1332	0.0953	0.0919	0.0636

Table 4.2: Gyroscope Parameters. Set:1.

	Real	Mean Value	RSM x10^{-3}	Mean Erorr x10^{-3}	RSM x10^{-3}	Worst case
γ_{yz}	0.0112	0.0110	0.8547	0.6392	0.5920	0.0099
γ_{zy}	-0.0211	-0.0210	0.4419	0.3468	0.2669	-0.0207
γ_{xz}	0.0040	0.0039	1.0630	0.9080	0.5266	0.0030
γ_{zx}	-0.0010	-0.0011	0.4102	0.3386	0.2302	-0.0011
γ_{xy}	0.0270	0.0270	0.8154	0.6375	0.4944	0.0252
γ_{yx}	0.0151	0.0155	0.7250	0.7315	0.3958	0.0166
s_x^g	0.8786	0.8785	0.4121	0.3366	0.2299	0.8790
s_y^g	0.9703	0.9704	0.4059	0.3353	0.2237	0.9701
s_z^g	1.0460	1.0460	0.4216	0.3410	0.2397	1.0460

Table 4.3: Absolute errors along the axis. Set:1.

(a) Accelerometer

	x-axis m/s^2	y-axis m/s^2	z-axis m/s^2
Uncalibrated	0.0842	0.0564	0.0635
Calibrated	0.0055	0.0056	0.0056

(b) Gyroscope

	x-axis (rad/s)	y-axis (rad/s)	z-axis (rad/s)
Uncalibrated	0.1043	0.1097	0.0345
Calibrated	0.0035	0.0039	0.0042

Table 4.4: Accelerometer divergence error. Set:1.

	Average error m/s^2(rad)	Max observed error $m/s^2(rad)$	Worst case average error $m/s^2(rad)$	Worst case max error $m/s^2(rad)$
Uncalibrated	0.0665	0.2133	0.0623	0.2098
	(0.0114)	(0.0226)	(0.0115)	(0.0240)
Calibrated	0.0056	0.0299	0.0056	0.0298
	(0.0009)	(0.0035)	(0.0009)	(0.0038)

Table 4.5: Gyroscope divergence error. Set:1.

	Average error m/s^2(rad)	Max observed error $m/s^2(rad)$	Worst case average error $m/s^2(rad)$	Worst case max error $m/s^2(rad)$
Uncalibrated	4.7125	9.2930	5.2859	8.5822
	(0.5494)	(0.5494)	(0.6029)	(0.6029)
Calibrated	0.2208	0.4469	0.5102	0.8597
	(0.0256)	(0.0256)	(0.0569)	(0.0569)

Starting from Tab. 4.1 and Tab. 4.2 it is possible to see that the average error commited estimating misalignment and scaling parameters of the accelerometer is of the order of 10^{-5} while all the others parameters are estimated under a error of the order of 10^{-4}. From Tab. 4.3, the absolute error commited along each axis of the accelerometer is improved of a factror 12.6 in mean, and for the gyroscope's axis the improvement is of a factor of 22.5 in mean. Finally from Tab. 4.4 and Tab. 4.5 it is possible to see that for what concrens accelerometer the divergence's magnitude is improved by a factor of 11.9 and the angular error by a factor of 12.7 while for the gyroscope the magnitude of the considered divergence is improved of a factor of 21.4 and the angular error of a factor of 21.9.

All these results refers to the first generetad set of distortion parameters, but very similar results are obtained in all the other thirtynine sets.

Finaly, in Fig. 4.10, 4.11, 4.12 and in Fig. 4.13, 4.14, 4.15 it is shown how the improvement due to calibration is significative. In this pictures are depicted six different rondomly choosen intervals referring to the six different sensors but referring to the same synthetic signal.

For what concerns accelerometer it is almost impossible to distinguish the real signal from the calibrated one. For the gyroscope we have very good results too but not so tight as for the accelerometer. This is due to the fact that, calibrating the accelerometer, an error is obviously made, however small, and as the results of this calibration are used to calibrate the gyroscopes, the error commited for the accelerometer is propagated to the calibration of the gyroscopes being added to the error inherently contained in the calibration of this latter sensor.

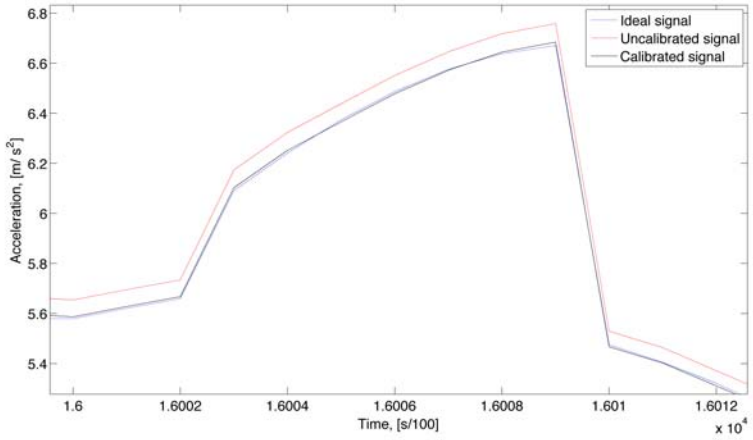

Figure 4.10: Calibration Improvement - Accelerometer x-axis.

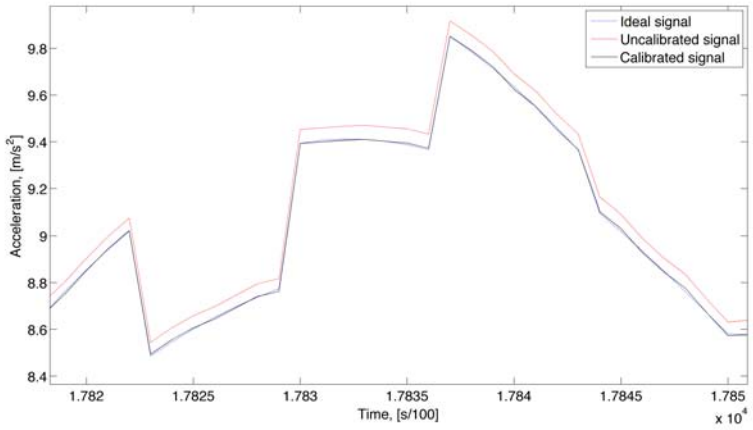

Figure 4.11: Calibration Improvement - Accelerometer y-axis.

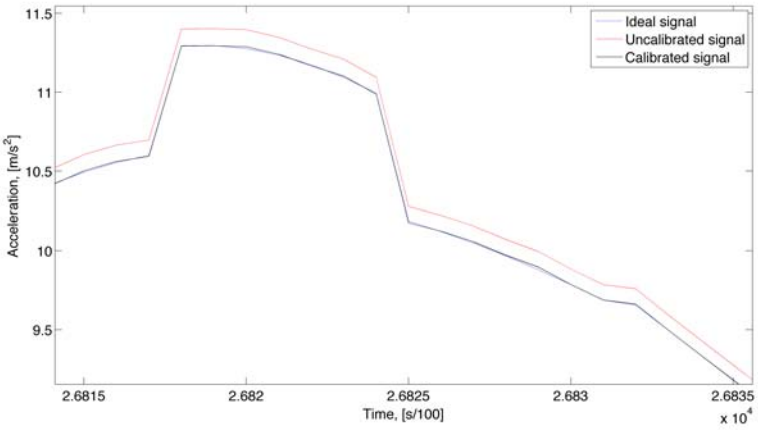

Figure 4.12: Calibration Improvement - Accelerometer z-axis.

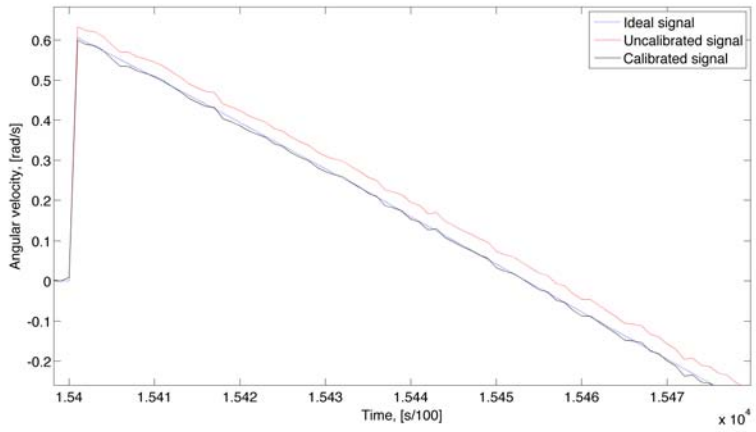

Figure 4.13: Calibration Improvement - Gyroscope x-axis.

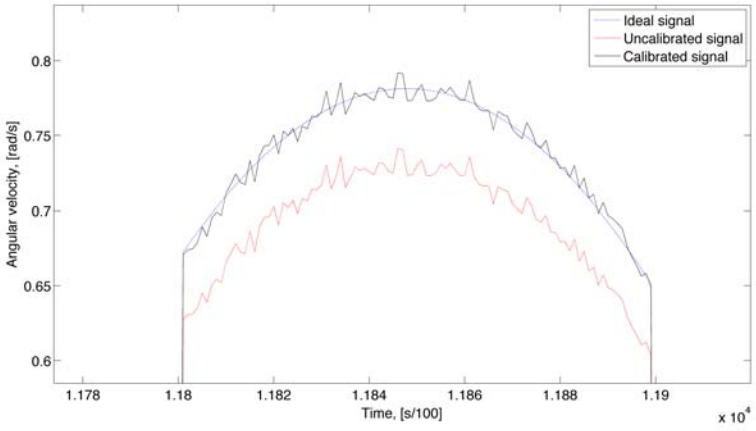

Figure 4.14: Calibration Improvement - Gyroscope y-axis.

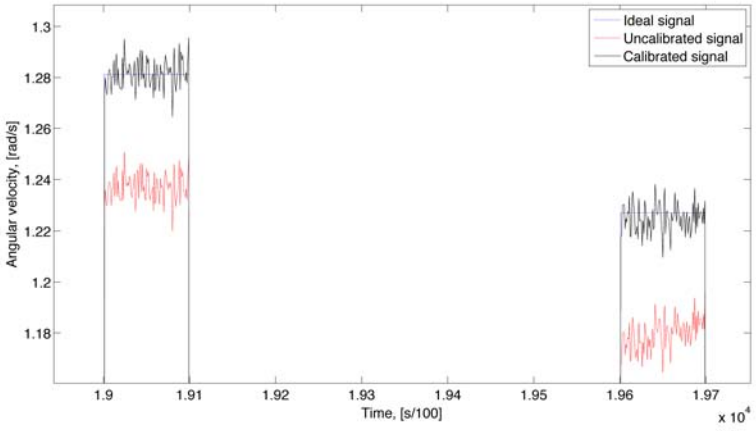

Figure 4.15: Calibration Improvement - Gyroscope z-axis.

4.2 Real Data Test

It is used an inertial measurement unit which can output raw unclibrated data and whose datasheet contains the calibration matrices we are estimating with our method. We compare the matrices we obtain by the uncalibrated data to the calibration matrices given by the datasheet. The real IMU we use to test the proposed algorithm is MTi by Xsens (the orange component in Fig. 3.3).

All specifications are given in Tab. 4.6, taken from [31]

Table 4.6: MTi specifications.

		rate of turn	acceleration	magnetic field	temperature
Unit		[deg/s]	[m/s^2]	[mGauss]	[°C]
Dimensions		3 axes	3 axes	3 axes	-
Full Scale	[units]	+/- 300	+/- 50	+/- 750	-55...+125
Linearity	[% of FS]	0.1	0.2	0.2	<1
Bias stability	[units 1σ]	1	0.02	0.1	0.5
Scale factor stability	[% 1σ]	-	0.03	0.5	-
Noise density	[units /√Hz]	0.05	0.002	0.5 (1σ)	-
Alignment error	[deg]	0.1	0.1	0.1	-
Bandwidth	[Hz]	40	30	10	-
A/D resolution	[bits]	16	16	16	12

where magnetometer noise density can be susceptible to electro-magnetic radiation and the alignment error is given after compensation for non-orthogonality, *i.e.* the error in the table is the error we have in the calibrated output.

4.2.1 Evaluation Metrics

As said before, we do not have any mechanical equipment capable of extremely precise maneuver so we consider as a ground truth the calibration matrices given in the MTi's datasheet.
Comparing the estimated matrices to the ones in the documentation is not properly an evaluation metric, but it permits us to evaluate if the calibration process is correct or not. We do not use the same matrics, the ones that does not require any external knowledge except the magnitude of the gravity vector, because using raw data, whose values has no fisical meaning, it has no sense evaluate the calibration results comparing data before and after calibration. In the next tables we have the calibration matrices as they give them in the datasheet.

Scaling factors are so big because they rapresent the factor that permit to reduce the quantized raw value given by the output, $output \in [0, 2^{16} - 1]$

(a) Scaling - Accelerometer

415	0.00	0.00
0.00	413	0.00
0.00	0.00	415

(b) Scaling - Gyroscope

4778	0.00	0.00
0.00	4758	0.00
0.00	0.00	4766

(c) Misalignment - Accelerometer

1.00	0.00	-0.01
0.01	1.00	0.01
0.02	0.01	1.00

(d) Misalignment - Gyroscope

1.00	-0.01	-0.02
0.00	1.00	0.04
-0.01	0.01	1.00

(e) Offset - Accelerometer

33123	33276	32360

(f) Offset - Gyroscope

32768	32466	32485

Table 4.7: MTi calibration parameters and offset.

to a fisical quantity. All the matrices are the inverse of the matrices we are actually estimating, so to compare our results we have to invert the estimated matrices. Actually, for the scale inverting the estimated matrices is correct but, for the misalignment, it is not sufficient. The device datasheet provides the factory calibrated misalignment matrices that align the accelerometers (AF) and gyroscopes (GF) frames to the body frame BF, while the estimated matrices align AF and GF to AOF. In order to compare our results with the results of the factory calibration, we need to know the matrix R_b that relates AOF to BF. Given R_b, we can express our calibration vectors in BF. R_b is the composition of three rotation, each one around one of the three axis of the chassis, and having each one a magnitude which we can recover from the misalignment matrix given in the datasheet (see section 2.2.1 for the reading of the misalignment matrix). Clearly, we have to multiply both the estimated misalignment matrices, the accelerometer one and the gyroscope one, by the same rotation matrix, because they both refers to the same orthogonal frame (AOF) which is misaligned to the chassis frame by angles just discussed.

From the datasheet we take and use only the data about the sensors offset. These values refer to the zero values of the sensors, and they do not refer to bias.

Finally we do not have anything to compare to the estimated bias for the accelerometer.

4.2.2 Real Data Test Results

Just to show an example of the trend of real signals, parts of them are pictured in Fig. 4.16 and in Fig. 4.17.

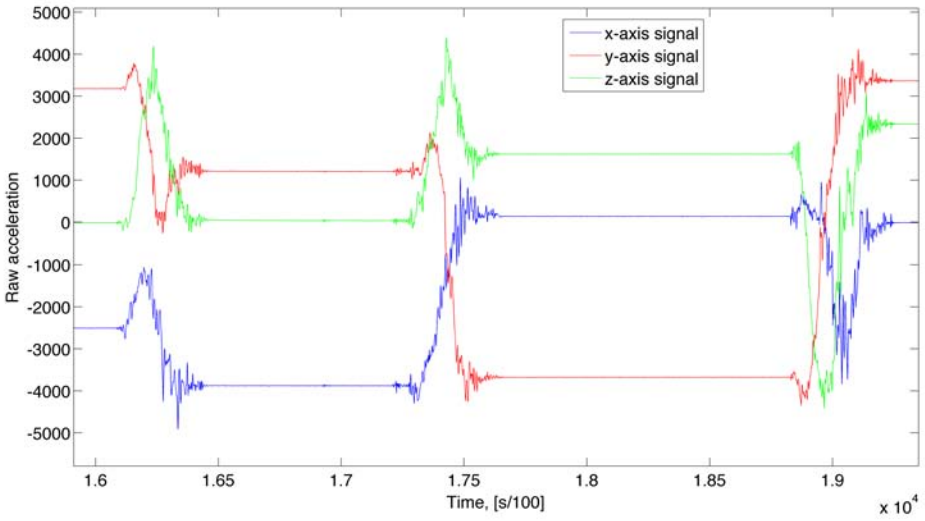

Figure 4.16: Example of real accelerometer raw signals.

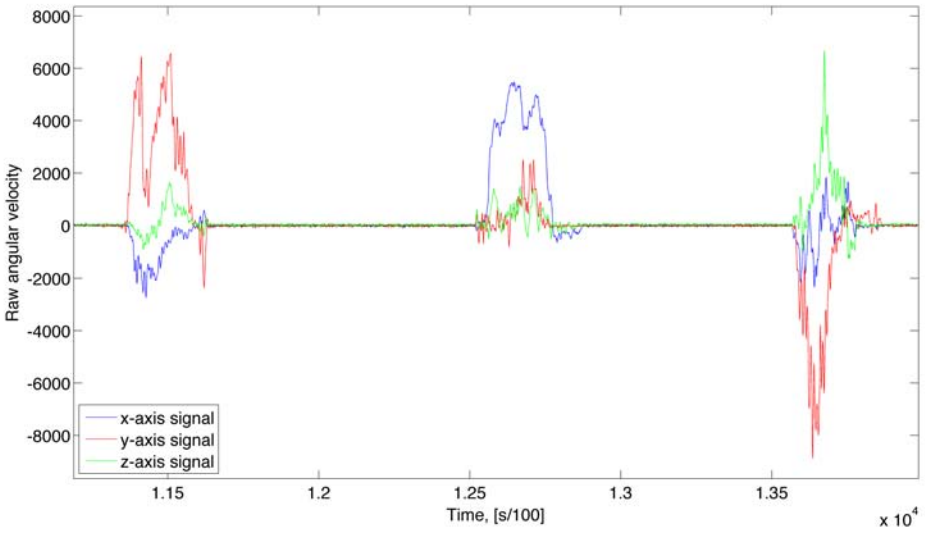

Figure 4.17: Example of real gyroscope raw signals.

First of all we demonstrate how the giroscope's signals changes after the

bias estimation via averaging of the signals themselves during the first long quasi static interval, Fig. 4.18.

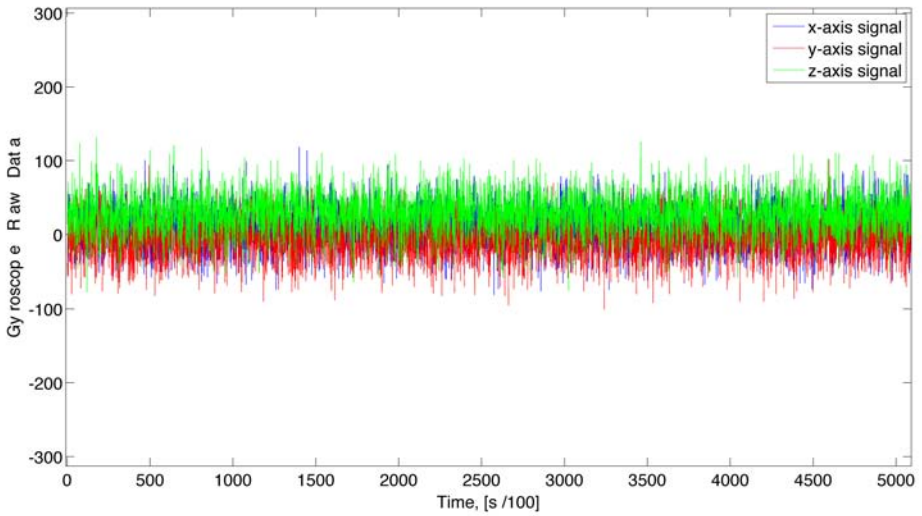

(a)

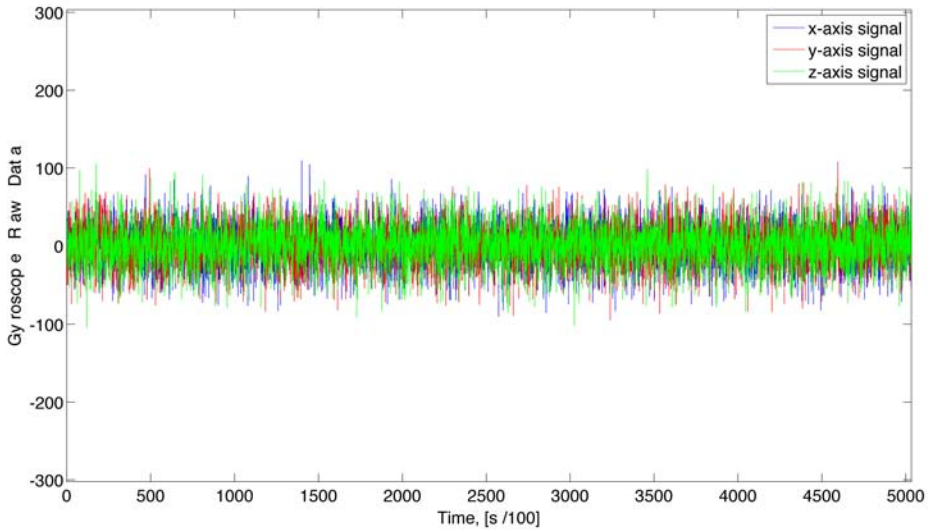

(b)

Figure 4.18: Bias remuval improvement. Before, *a*), and after, *b*), bias remuval.

The real dataset was acquired as described in Fig. 1.1, with an initial static period of about 50 seconds, followed by a set of 37 rotations separated

by static intervals of 2-4 seconds. As initial guess for the optimization the ideal values are used for the accelerometer, that are (see Eq. 3.2):

$$\begin{bmatrix} 0 & 0 & 0 & 1 & 1 & 1 & 0 & 0 & 0 \end{bmatrix}. \tag{4.3}$$

While for the gyroscope are used (see Eq. 3.6):

$$\begin{bmatrix} 0 & 0 & 0 & 0 & 0 & 0 & \frac{1}{r} & \frac{1}{r} & \frac{1}{r} \end{bmatrix}, \; r = \frac{(2^n - 1)}{2y} \tag{4.4}$$

where n is the numbers of bit of the A/D converter, and the gyroscope full-scale from datasheet is [-y, +y] rad/s.

(a) Estimated Scaling - Acc

414.41	0	0
0	412.05	0
0	0	414.61

(b) Estimated Scaling - Gyro

4778.0	0	0
0	4764.8	0
0	0	4772.6

(c) Estimated Misalignment - Acc

1.0000	-0.0066	-0.0110
0.0102	1.0001	0.0114
0.0201	0.0098	0.9998

(d) Estimated Misalignment - Gyro

0.9998	-0.0149	-0.0218
0.0003	1.0007	0.0433
-0.0048	0.0121	1.0004

Table 4.8: MTi estimated calibration parameters.

The calibration obtained, Tab. 4.8, is absolutely comparable to the calibration parameters given in the datasheet, see Tab. 4.7. Moreover, it is important to point out that in the results it is implicitly included an error that can't be attributed to the calibration method. This is the propagated error caused by the IMU's datasheet rounded values (Tab. 4.7c) used when R_p is computed. In spite of this problem, the results obtained are very close to datasheet's parameters.

Chapter 5

Conclusions

"Take risks:
if you win, you will be happy;
if you lose you will be wise."

Peter Kreeft

This thesis presents a calibration method for a IMU that requires neither any specially designed equipments nor the long and laborious procedures for data sampling. The procedure for the collection of data allows the sensor to be moved by hand, and only requires a few minutes of arbitrary rotations with intermittent pauses. Also a protocol is given, which a user should follow in order to calibrate his IMU. A robust integration tecnique is used while exposed procedure does not require any parameter tuning. Simulations gives excellent results, while the calibration of the real IMU is very good too. The most significative part of the errors in the real IMU calibration comes from the rounded values of the angle we extract from datasheet.

A scientific paper based on this work has been submitted to ICRA 2014: the most important robotics conference in the world.

5.1 Future Works

More robust tests can be done on real IMUs, also testing the method on different kinds of IMU, e.g. IMUs working at different sampling rates. Testing uncalibrated IMUs that gives in output wrong fisical quantities instead of quantized values, permits to employ the metrics used in this thesis for the evaluation of simulations' results (i.e. the divergence between the magnitude

of the gravity vector and the acceleration sensed by the IMU standing static and so on).

After these studies, the protocol and the algorithm can be optimized specifically for particular IMUs, such as a defined smartphone's IMU (e.g. defining a specified protocol and implementing an optimized algorithm in *Objectice-C*, [33], to calibrate the specific IMU contained in the iPhone 5s, [34]).

Finally considering that are already aviable smartphones with build-in thermometer (like the Galaxy S4, [35]) some studies can be perfomed to take into account temperature effects on the calibration parameters and in such a way improve the reliability of the obtained calibration.

Bibliography

[1] Kubelka, Vladimir and Reinstein, Michal, Proc. of. IEEE International Conference on Robotics and Automation (ICRA), pp. 599-605, *Complementary filtering approach to orientation estimation using inertial sensors only.*, 2012.

[2] Hamel, Tarek and Mahony, Robert E., Proc. of. IEEE International Conference on Robotics and Automation (ICRA), pp. 2170-2175, *Attitude Estimation on SO[3] based on Direct Inertial Measurements.*, 2006.

[3] Konstantine Tsotsos and Alberto Pretto and Stefano Soatto, IEEE-RAS International Conference on Humanoid Robots, pp. 704-711, *Visual-Inertial Ego-Motion Estimation for Humanoid Platforms*, 2012.

[4] Konolige, K. and Agrawal, M., IEEE Transactions on Robotics, 24-5 pp. 1066-1077 *FrameSLAM: From Bundle Adjustment to Real-Time Visual Mapping*, Oct 2008.

[5] M. Li and B.H. Kim and A. I. Mourikis, Proceedings of the IEEE International Conference on Robotics and Automation, pp. 4697-4704, *Real-Time Motion Estimation on a Cellphone using Inertial Sensing and a Rolling-Shutter Camera*, May 2013.

[6] XSens, `http://www.xsens.com/`.

[7] J.C. Lotters and J. Schipper and P.H. Veltink and W. Olthuis and P. Bergveld, Sensors and Actuators A: Physical, 68 1-3pp. 221-228, *Procedure for in-use calibration of triaxial accelerometers in medical applications*, 1998.

[8] W. Fong and S. Ong and A. Nee, Measurement Science and Technology, vol. 19, p. 085202, *Methods for in-field user calibration of an inertial measurement unit without external equipment*, 2008.

[9] Rogers, R.M., American Institute of Aeronautics and Astronautics, AIAA education series, *Applied Mathematics in Integrated Navigation Systems*, 2003.

[10] Chatfield, Averil B., Reston, VA. American Institute of Aeronautics and Astronautics, Inc., Progress in astronautics and aeronautics, *Fundamentals of high accuracy inertial navigation*, 1997.

[11] Hall, J. J. and Williams II, R. L., Journal of Robotic System, 17 11 pp. 623-632, *Inertial measurement unit calibration platform*, 1998.

[12] Kim, A. and Golnaraghi, M.F., Position Location and Navigation Symposium, 2004. PLANS 2004, pp. 96-101, *Initial calibration of an inertial measurement unit using an optical position tracking system*, 2004.

[13] Nebot, Eduardo Mario and Durrant-Whyte, Hugh F., Journal of Robotic Systems, 16 2 pp. 81-92, *Initial calibration and alignment of low-cost inertial navigation units for land vehicle applications.*, 1999.

[14] Skog I. and Händel P., Proc. 17th IMEKO World Congress (Rio de Janeiro, pages 17–22 ,September 2006), *Calibration of a MEMS inertial measurement unit*, 2006.

[15] , Syed Z F, Aggarwal P., Goodall C., Niu X. and El-Sheimy N. *A new multi-position calibration method for MEMS inertial navigation systems*, 2007
Meas. Sci. Technol. 18 1897–907.

[16] Cheuk, Chi Ming and Lau, Tak Kit and Lin, Kai Wun and Liu, Yunhui, in Proc. of International Conference on Control, Automation, Robotics and Vision, *Automatic Calibration for Inertial Measurement Unit*, 2012.

[17] Myung Hwangbo and Jun-Sik Kim and Takeo Kanade, IEEE Transactions on Robotics, 29 2 pp. 493-507, *IMU Self-Calibration Using Factorization*, 2013.

[18] `http://www.xsens.com/en/general/mti`.

[19] Huff M.A., *MEMS Manufacturing, The MEMS Exchange* , 1999, Position Paper, U.S.A. Reston, Virginia.

[20] `https://www.memsnet.org/about/what-is.html`

[21] Benjamin Peter, *Development of an Automatic IMU Calibration System*, Spring Semester 2011,
Master Thesis, Autonomous Systems Lab, Eidgenössische Technische Hochschule Zürich, ETH.

[22] Samuel Fux *Development of a planar low cost Inertial Measurement Unit for UAVs and MAVs*, Spring Term 2008,
Master Thesis, Autonomous Systems Lab, Eidgenössische Technische Hochschule Zürich, ETH.

[23] Agostino Martinelli, *Visual-Inertial Structure from Motion Observability*, Mars 2013,
Thèmes COG et NUM Rapport de recherche number 8272

[24] Eagle S. Jones and Stefano Soatto , *Visual-inertial Navigation, Mapping and Localization: A Scalable Real-Time Approach*, 23rd September 2010,
Intl. J. of Robotics Research.

[25] Andrle, Michael and Crassidis, John, in Proc. of AIAA/AAS Astrodynamics Specialist Conference, *Geometric Integration of Quaternions*, 2012.

[26] Sabatini, Angelo M., Measurement Science and Technology, 17 11 pp. 2980-2988, *A wavelet-based bootstrap method applied to inertial sensor stochastic error modelling using the Allan variance*, 2006.

[27] J.C. Hung, J.R. Thacher and H.V. White, *Calibration of accelerometer triad of an IMU with drifting Z-accelerometer bias*, in Proc. NAECON 1989,
IEEE Aerospace and Electronics Confer- ence, 22–26 May. 1989, vol. 1, pp. 153 – 158.

[28] Christopher Jekeli, "Inertial Navigation Systems with Geodetic Applications", 2001,
Walter de Gruyter.

[29] Erik B. Dam, Martin Koch, Martin Lillholm, *Quaternions, Interpolation and Animation*, July 17, 1998,
Technical Report DIKU-TR-98/5, Department of Computer Science, University of Copenhagen, Denmark.

[30] Saxena A., Gupta G., Gerasimov V. and Ourselin S., *In use parameter estimation of inertial sensors by detecting multilevel quasi-static state*,

2005,
Lect. Notes Comput. Sci. 3684 595–601.

[31] Xsens Technologies B.V.: *MTi and MTx Low-Level Communication Documentation* September 20, 2006,
Document MT0101P, Revision F.

[32] `http://ww2.ptgrey.com/stereo-vision/bumblebee-2`

[33] `https://developer.apple.com/library/mac/navigation/`

[34] `http://www.apple.com/iphone-5s/`

[35] `http://www.samsung.com/it/promotions/galaxys4/`

Acknowledgements

Dedico questo lavoro e il risultato finale del mio percorso di studi alla mia **famiglia**, le mie origini, di cui sono fiero e orgoglioso. Ringrazio pertanto i miei genitori, **Monica** e **Costantino**, e mia sorella **Elisa**, i quali hanno contribuito tutti e tre a questo risultato condividendo con me le loro esperienze dandomi così spunti di riflessione e molte possibilità di crescita. Grazie intolre per l'affetto e il sostegno che non sono mai venuti meno.

Ringrazio tutti coloro isieme ai quali sono cresciuto in questi tre anni, che ho conosciuto in questo ambiete e non e che sono diventati dei grandi, grandissimi amici. Un sincero grazie**Alessio**, **Tommaso**, **Fabio**, **Marco**, **Enea**, per le loro sraordinarie e variegate personalità, perchè ognuno di loro, con il suo modo di essere mi ha data tanto.
Grazie agli amici di sempre, **Riccardo**, **Sofia** e **Francesco**, che sono sempre stati presenti, nonostante le ore che ho sottratto loro per lo studio.

Ringrazio poi **Stefano G.**. Presso l'Università di Padova non esiste ancora la figura del *Mentor*, come figura anziana che segue e consiglia uno studente più giovane, ma ho avuto la fortuna di incontrarlo il primo anno e da quel giorno le chiaccherate fatte di tanto in tanto sono state davvero fondamentali per molte delle scelte fatte a livello accademico.
Ringrazio **Alberto**, per avermi iniziato all'affascinante e sconfinato mondo della ricerca, per il grande aiuto e sostegno teorico e morale datomi durante lo svolgimento di questo lavoro.
Ringrazio anche tutti i dottori e dottorandi del laboratorio di robotica autonoma, **Sefano M.**, **Mauro**, **Matteo**, **Filippo**, **Elisa** e **Francesco**, per le chiaccherate fatte sul loro lavoro, i pasti condivisi, e per avermi fatto capire che la ricerca come me la immaginavo io esiste anche in Italia.
Un ringraziamento al **professor Menegatti**, per aver creduto in me sin dal primo colloquio.

Grazie **Carlotta** per ogni volta che hai acceso la lucina, per ogni passo fatto fianco a fianco, e per tutto quello che ogni giorno, dal più indaffarato al più spensierato, tu sei per me.